



Heterocellular 3D scaffolds as biomimetic to recapitulate the tumor microenvironment of peritoneal metastases *in vitro* and *in vivo*



Emiel De Jaeghere ^{a,b,1}, Elly De Vlieghere ^{a,b,1}, Jasper Van Hoorick ^c, Sandra Van Vlierberghe ^c, Glenn Wagemans ^a, Leen Pieters ^d, Elodie Melsens ^e, Marleen Praet ^f, Jo Van Dorpe ^{b,f}, Matthieu N. Boone ^g, Rouba Ghobeira ^h, Nathalie De Geyter ^h, Marc Bracke ^{a,b}, Christian Vanhove ^{b,i}, Sara Neyt ^j, Geert Berx ^{b,k}, Bruno G. De Geest ^{b,l}, Peter Dubrule ^c, Heidi Declercq ^{b,d}, Wim Ceelen ^{b,e}, Olivier De Wever ^{a,b,*}

^a Laboratory Experimental Cancer Research (LECR), Ghent University, De Pintelaan 185, 9000 Ghent, Belgium

^b Cancer Research Institute Ghent (CRIG), Ghent University, De Pintelaan 185, 9000 Ghent, Belgium

^c Polymer Chemistry & Biomaterials Group, Centre of Macromolecular Chemistry, Ghent University, Krijgslaan 281, S4-Bis, 9000 Ghent, Belgium

^d Department of Basic Medical Sciences, Ghent University, De Pintelaan 185, 9000 Ghent, Belgium

^e Experimental Surgery Lab, Department of Surgery, Ghent University, De Pintelaan 185, 9000 Ghent, Belgium

^f Department of Pathology, Ghent University Hospital, Ghent University, De Pintelaan 185, 9000 Ghent, Belgium

^g Department of Physics and Astronomy, Ghent University, Proeftuinstraat 86, 9000 Ghent, Belgium

^h Department of Applied Physics, Research Unit Plasma Technology (RUPT), Ghent University, Sint-Pietersnieuwstraat 41, B4, 9000 Ghent, Belgium

ⁱ Institute Biomedical Technology, Ghent University, De Pintelaan 185, 9000 Ghent, Belgium

^j MOLECUBES NV, Ottergemsteenweg-Zuid 808, 325 Ghent, Belgium

^k Department of Biomedical Molecular Biology, Unit of Molecular and Cellular Oncology, Inflammation Research Center, VIB, Technologiepark Zwijnaarde 927, 9052 Ghent, Belgium

^l Department of Pharmaceutics, Ghent University, Ottergemsteenweg 460, 9000 Ghent, Belgium

ARTICLE INFO

Article history:

Received 24 October 2017

Received in revised form

20 December 2017

Accepted 21 December 2017

Available online 23 December 2017

Keywords:

Tissue engineering

Hybrid scaffolds

Tumor microenvironment

Hydrogels

Cancer-associated fibroblasts

Biomimetics

ABSTRACT

Peritoneal metastasis is a major cause of death and preclinical models are urgently needed to enhance therapeutic progress. This study reports on a hybrid hydrogel-polylactic acid (PLA) scaffold that mimics the architecture of peritoneal metastases at the qualitative, quantitative and spatial level. Porous PLA scaffolds with controllable pore size, geometry and surface properties are functionalized by type I collagen hydrogel. Co-seeding of cancer-associated fibroblasts (CAF) increases cancer cell adhesion, recovery and exponential growth by *in situ* heterocellular spheroid formation. Scaffold implantation into the peritoneum allows long-term follow-up (>14 weeks) and results in a time-dependent increase in vascularization, which correlates with cancer cell colonization *in vivo*. CAF, endothelial cells, macrophages and cancer cells show spatial and quantitative aspects as similarly observed in patient-derived peritoneal metastases. CAF provide long-term secretion of complementary paracrine factors implicated in spheroid formation *in vitro* as well as in recruitment and organization of host cells *in vivo*. In conclusion, the multifaceted heterocellular interactions that occur within peritoneal metastases are reproduced in this tissue-engineered implantable scaffold model.

© 2017 Elsevier Ltd. All rights reserved.

1. Introduction

Peritoneal metastases originating from ovarian and colorectal

cancer are common and are increasingly regarded as a treatable locoregional progression of disease, rather than a manifestation of systemic disease. This new insight resurged an interest in intraperitoneal chemotherapy after surgical cytoreduction [1]. Since reintroduction of intraperitoneal chemotherapy, there is a trend toward long-term survival and even disease cure, with reported 5-year survival rates as high as 50% [2,3]. Although intraperitoneal

* Corresponding author.

E-mail address: Olivier.dewever@ugent.be (O. De Wever).

¹ Emiel De Jaeghere and Elly De Vlieghere contributed equally.

chemotherapy has encouraging efficacy, its major limiting factor is the very poor tissue penetration. Accordingly, there is limited survival benefit from intraperitoneal chemotherapy for patients with residual tumor nodules exceeding the size of 5.0 mm for ovarian cancer and 2.5 mm for colorectal cancer [4,5]. Another important point to be emphasized is that the peritoneal tumor microenvironment, mainly composed of cancer-associated fibroblasts (CAF) and their extracellular matrix, also contributes to therapy resistance by inducing interstitial hypertension and scavenging chemotherapy, among others [6,7]. To further improve intraperitoneal chemotherapy's potential, preclinical peritoneal metastasis models should more closely mimic the tumor microenvironment of bulky residual disease ($>5.0\text{ mm}, \pm 100\text{ mm}^3$).

Several xenograft models are currently used to model peritoneal metastases and can be grouped into three categories [8]. 1) The intraperitoneal injection of suspended cancer cells (cancer cell line or patient-derived) into the abdominal cavity has been a useful and widely used tool to establish peritoneal metastases. For some cancer cell lines, this procedure yields high tumor take and dissemination rates and permits fast tumor growth, and as such, replicates peritoneal metastases in patients quite well macroscopically. The countless tumor nodules are ideally suited to study the processes of peritoneal dissemination, but their size is considered too small ($<1\text{ mm}$) to be relevant for intraperitoneal drug applications for bulky residual disease [9–11]. 2) In contrast, the sub-peritoneal injection of cancer cells initiates a single, localized, large tumor nodule (due to controlled cancer cell transfer), whereas additional peritoneal metastases occur rarely or not at all. This technique, however, should be regarded as an ectopic model where the metastasis is established at the wrong side of the peritoneal layer and is not directly exposed to the abdominal cavity [12,13]. 3) In a tumor transplant model, human cancer cells are subcutaneously injected into a donor mouse. Once the tumor grows to an appropriate size, it is engrafted orthotopically into the abdominal cavity of another host animal (acceptor) [14]. A disadvantage of this model is that the transplant tumor generally fails both to elicit an efficient infiltration of blood vessels and to initiate vascular anastomoses between graft and recipient blood vessels.

While much has been learned with the aforementioned models, they do not fully recapitulate what is observed in the cognate peritoneal metastasis microenvironment. In fact – in these xenografts – the bulk of tumor comprises only cancer cells, while CAF, extracellular matrix, immune cells and blood vessels are only a minor component of the mass. Obviously, the presence of a suitable microenvironment is considered to be important to assess tumor response to intraperitoneal (or intravenous) chemotherapy [15]. Continued development in the fields of cancer systems biology, 3D modeling, biomaterials and tissue engineering provides new opportunities to design more patient-relevant metastasis models. For instance, tissue engineering of the pre-metastatic niche [16] and bone metastases [17] has been successful but – to the best of our knowledge – no attempts have yet been made to engineer a bio-mimetic of a peritoneal metastasis that can provide an advanced technology platform for both *in vitro* and *in vivo* experiments.

The present work aimed to employ hybrid hydrogel-polylactic acid (PLA) scaffolds to combine the advantages of both (bio)materi-als and to overcome the challenges discussed above, including size and geometry requirements, participation of the tumor microenvironment, efficient engraftment and successful cell colonization. 3D printing enables fabrication of scaffolds – “peritoneal metastases” – of practically any desired dimension and geometry. Above all, scaffolds are highly porous, which permits cellular infiltration and ensures interaction with host tissue, including angiogenesis and inflammation, both of which are important to metastasis and drug resistance [18]. The rigid and mechanical

stable nature of the PLA scaffolds allows implantation into the peritoneum of an appropriate host animal. PLA is considered to be biocompatible, but both biochemical surface modification by gel-MOD coating and the employment of a type I collagen hydrogel provide a more matrix- and cell-interactive nature to the construct. Another key point is that CAF are drivers of peritoneal metastasis [19]; the addition of CAF to cancer cells in a type I collagen hydrogel stimulated cancer cell growth and invasion in ovarian and colorectal cancer models [19,20].

In summary, we examined the potential of hybrid hydrogel-PLA scaffolds and CAF to support the *in vitro* engineering of the tumor microenvironment of bulky peritoneal metastases and the subsequent implantation of this tissue-engineered construct to serve as an *in vivo* technology platform for intraperitoneal xenografts.

2. Methods

2.1. Scaffold development

Scaffolds were produced using fused deposition modeling (FDM) as reported in a similar fashion earlier by Van Hoorick et al. [21] In brief, scaffolds were fabricated using a transparent Poly (L-lactic acid) (PLA, Mn: 132400 g/mol and Mw: 166500 g/mol) filament (Velleman, Gavere, Belgium) in combination with an Ultimaker 1 device (Ultimaker, Geldermalsen, Netherlands). The pore size (550 μm), printing temperature (210 °C), number of layers ($n=20$) and layer height (200 μm) were transferred into a G-code using an in-house developed scaffold generator v1.8 program (Ghent University) written in Visual Basic for Applications in Microsoft Excel 2010. Next, the G-codes driving the circular printing nozzle (diameter 400 μm) were transferred to the Ultimaker 1 using Cura 13.06.4 software (Ultimaker, Geldermalsen). As a result, porous PLA slabs of 50 mm (length) \times 50 mm (width) \times 4 mm (height) with a lay down pattern of 0/90° were deposited at 11 mm/s at 210 °C in meander. After manufacture, slabs were cut with a circular metallic puncher to obtain cylindrical scaffolds with a diameter of 6 mm (Fig. 1A). The mechanical properties of the scaffolds were determined using a Tinius-Olsen 5ST tensile tester using a 500 N load cell. Measurements were performed up until 400 N load and analyzed using Horizon software.

2.2. Scaffold surface modification

The cylindrical scaffolds were subjected to an argon plasma using a FEMTO plasma reactor version 3 (Diener Electronic, Ebhausen, Germany) for 30 s at a pressure of 0.8 mbar and a power of 100 W. Next, the scaffolds were exposed to ambient atmosphere for 20 min to allow for the reaction of free radicals on the surface with oxygen to form (hydro)peroxides, as previously reported [22]. To perform the coating, the plasma activated cylindrical PLA scaffolds were immersed into a 2 w/v% gel-MOD (DS 97, see supplementary materials and methods) solution in double distilled water, containing 2 mol% Irgacure 2959 (BASF, Antwerp, Belgium) (relative to the amount of methacrylamides starting from a stock solution containing 8 mg/ml Irgacure 2959) at 40 °C under continuous magnetic stirring. Next, a 5-min vacuum treatment was performed to allow sufficient intrusion of the solution throughout the pores of the scaffolds. Afterwards, the scaffolds were placed on glass slides and exposed to UV-A irradiation (356 nm, 8 mW/cm²) for 60 min to induce covalent crosslinking. Finally, the scaffolds were sterilized by ethylene oxide (AMSCO Eagle 3017, Steris, Antwerp, Belgium) (Fig. 1A).

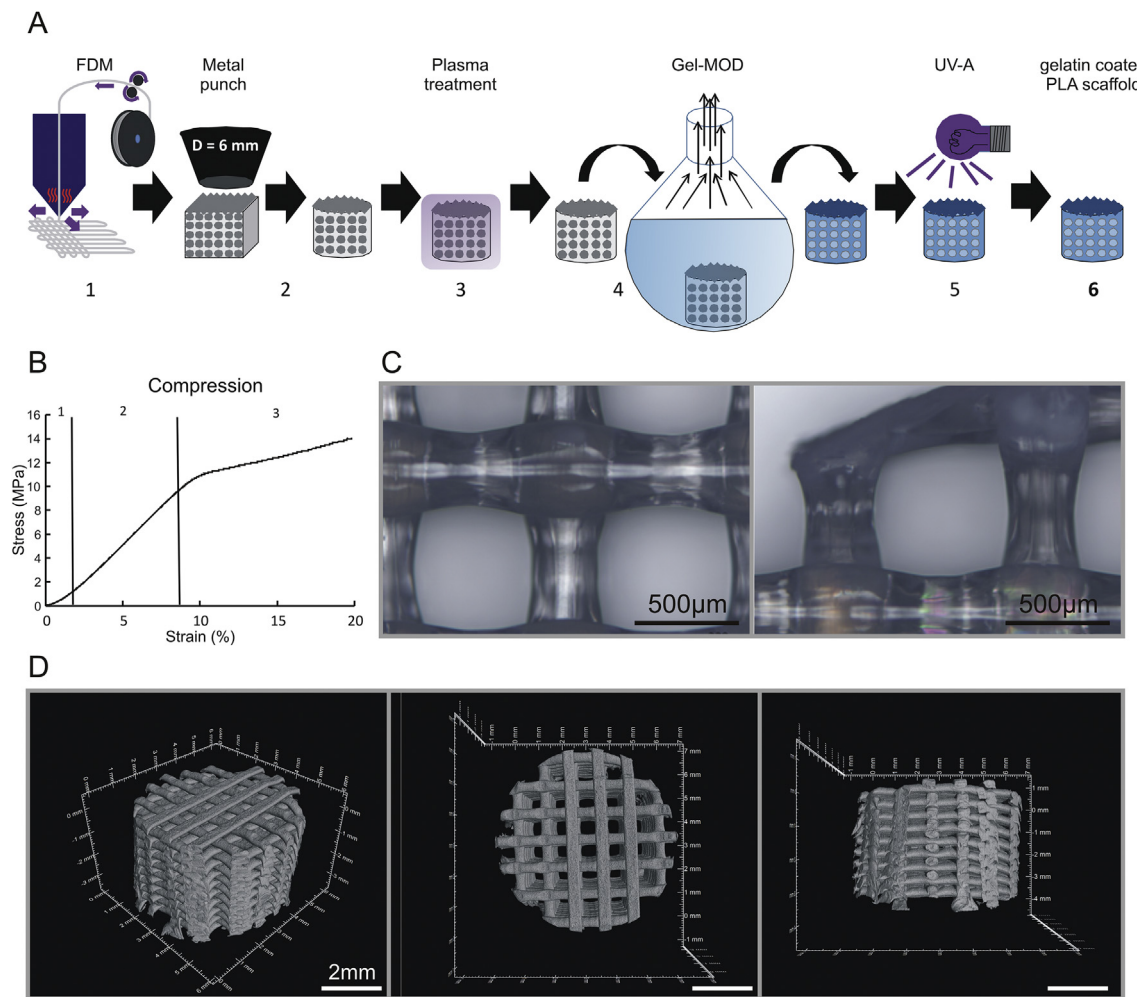


Fig. 1. PLA scaffolds. A) Workflow of scaffold production: a cuboid scaffold slab is obtained via fused deposition modeling (1); cylinder ($d = 6$ mm) is punched from the slab (2); surface is activated via plasma treatment (3); introduction of gelatin coating by immersing the scaffold in 2 w/v% solution containing 2 mol% Irgacure 2959 photoinitiator, intrusion in the pores is facilitated by vacuum treatment (4); crosslinking of gel-MOD coating using UV-A treatment (365 nm) (5); end product scaffold ready for cell seeding (6). B) Stress-strain plot obtained from compression test: 1) force exhibiting area where contact with scaffold and tensile tester is established; 2) elastic deformation area used to calculate E-modulus; 3) plastic region of deformation. C) Top view optical microscopy image of scaffold. D) μ CT reconstruction of scaffold: isometric view (left), top view (center) and cross section (right).

2.3. Characterization of PLA scaffolds

The dimensions (height, diameter, pore size and strut thickness) of the scaffolds were measured by microscopy and μ CT. The porosity was calculated based on data collected by μ CT and helium pycnometry. Mechanical properties of the PLA scaffolds were obtained using compression tests with compressive forces up to 400 N. More detailed information can be found in the supporting experimental section.

2.4. Cell lines

Isolation, characterization and culture of human colorectal CAF were previously described [9,20,23]. SK-OV-3 is a human ovarian cancer cell line (ATCC number: HTB-77). HCT-8/E11 is a human colon cancer cell line (ATCC number: CCL-244). SK-OV-3 Luc and HCT-8/E11 Luc cells were prepared by pFL4.76 plasmid transfection and selection (Promega). SK-OV-3 Luc eGFP and CAF tdTomato were obtained by retroviral transduction of pLenti6(Blast)-eGFP-V5 and pLenti6(Blast)-tdTomato-V5 vectors respectively. All cell lines were maintained in Dulbecco's modified Eagle's medium (DMEM)

(Invitrogen) supplemented with 10% FBS and antibiotics (penicillin/streptomycin) and incubated at 37 °C with 10% CO₂ in air. Authenticity of ATCC cell lines was confirmed by short tandem repeat profiling. All cell lines tested negative for mycoplasma contamination.

2.5. Tumor/control scaffold seeding procedure

Tumor scaffolds were obtained by seeding PLA scaffolds with a combination of CAF and cancer cells. Seeding density was optimized at 2×10^6 cancer cells (either SK-OV-3 Luc (eGFP) or HCT-8/E11 Luc) and 8×10^6 CAF (CAF tdTomato). For each scaffold, the pelleted cells were suspended in 0.4 ml 0.2% type I collagen suspension at room temperature. 1 ml 0.2% collagen suspension contains: 454 μ l collagen type I (Bioconnect, 100mg/22.68 ml), 182 μ l CMF-HBSS, 72 μ l MEM10X, 72 μ l NaHCO₃, 20 μ l NaOH 1 M and 200 μ l culture medium [24]. Prior to seeding, scaffolds were incubated at 37 °C for 1 h in a 24-well culture plate. During seeding, temperature was maintained on a plate heater set at 37 °C. Seeding was performed in a 2-ml tube by pipetting the collagen-suspended cells onto the scaffolds. Passive percolation at atmospheric pressure

for 20s was followed by a 20-s vacuum treatment (N816·3 KN.18 diaphragm pump, KNF, Aartselaar, Belgium). The seeded scaffolds were subsequently positioned in a 24-well culture plate. Finally, the seeded scaffolds were inverted after 30 min to reduce gravity-induced remodeling of the collagen suspension and cell distribution inside the scaffold (Fig. 2A). Cell-free scaffolds have undergone the same seeding procedure with collagen only, without cells, and are referred to as control scaffolds. After incubation overnight in a humidified 10% CO₂ atmosphere at 37 °C, scaffolds were maintained in 2 ml of Dulbecco's modified Eagle's medium (DMEM) (Invitrogen) supplemented with 10% FBS and antibiotics (penicillin/streptomycin). Medium was refreshed twice a week.

2.6. In vitro viability and organization of tumor scaffolds

Bioluminescence imaging (BLI) was applied to longitudinally monitor the viability and proliferation of the cancer cells independently from the CAF, as only cancer cells were transferred with the luciferase gene. Cellular viability was assessed using LIVE/DEAD staining. Although it provides information about viability, it cannot distinguish cancer cells from CAF. Cellular organization within the tumor scaffolds was observed using fluorescently labeled cells (CAF tdTomato and SK-OV-3 Luc eGFP) and Haematoxylin&Eosin stainings (H&E) on paraffin-embedded sections. More detailed information can be found in the supporting experimental section. Scaffold seeding and viability monitoring was performed multiple times (>4), 2 representative experiments are shown.

2.7. Luminex

On days 1, 3 and 8 of HCT-8/E11 and CAF cultures, aliquots of supernatant were collected and subjected to secretome analysis using Luminex multiplex arrays by Eve Technologies (Calgary, AB Canada). Discovery assays used are Human Cytokine Array/Cytokine Array 65-Plex Panel (HD65) and Human Angiogenesis Array & Growth Factor 17-plex Array (HDAGP17). All samples were assayed at least in duplicate and prepared standards were included in all runs. In the analysis, baseline media analyte levels were accounted for.

2.8. In vivo experiments

Animal experiments were carried out in accordance with the regulatory guidelines of the Ethics Committee of the Ghent University Hospital. A total of 6 female athymic Swiss Nu/nu mice (Charles River) at 6 weeks of age were used for xenograft studies and kept in standard housing conditions with water and food *ad libitum*. Tumor scaffolds ($n = 6$), seeded with SK-OV-3 Luc eGFP and CAF tdTomato 3 weeks prior to intraperitoneal implantation, were sutured to the parietal peritoneum of the right lower abdominal quadrant. As a control, four of these mice were sutured cell-free/control scaffolds ($n = 4$) to the parietal peritoneum of the left lower abdominal quadrant. Cancer cell growth was monitored weekly by bioluminescence imaging. Blood vessel infiltration was *in vivo* visualized and quantified by contrast-enhanced μCT using the X-Cube cone beam μCT (MOLECUBES NV, Ghent, Belgium) at 4 weeks post implantation (4/6 mice). At this time point, two mice were sacrificed and the implanted scaffolds were harvested for H&E and immunohistochemical stainings. At the endpoint, 12–14 weeks post implantation, *in vivo* and *ex vivo* contrast-enhanced μCT scans were performed (4/6 mice). Finally, the tumor and control scaffolds were paraffin embedded for H&E stainings (Fig. 3A and B). Data is shown from two independent experiments. More detailed information can be found in the supporting experimental section. The traditional mouse model was obtained by intraperitoneal

injection of a suspension of 1×10^6 SK-OV-3 Luc cells (in 250 μl saline). Small tumors had already spread widely throughout the peritoneal cavity after 6 weeks. These tumors were paraffin embedded for H&E staining.

2.9. Statistics

Statistical analysis was performed using GraphPad Prism 5.03. Blood vessel infiltration was analyzed by Mann-Whitney U one-tailed tests, correlations were analyzed with Spearman's rank correlation coefficients. Differences with $p < .05$ were considered statistically significant.

3. Results

3.1. Synthesis and characterization of the PLA scaffold

Polymer-based scaffolds, such as polylactic acid (PLA) scaffolds, ensure mechanical stability, high porosity and that size and shape requirements are met. Fused deposition modeling (FDM), a manufacturing technology that lays down molten polymer in additive layers with a 3D printer, is applied to generate scaffolds from PLA filaments. The surface of the PLA scaffolds is coated with gelatin to increase cellular interactivity. In short, scaffolds are argon plasma treated and consequently dip coated in a 2 w/v% gel-MOD (cross-linkable gelatin) solution containing 2 mol% Irgacure 2959 which is cross-linked through UV-A irradiation (Fig. 1A). The stiffness of the PLA scaffolds is assessed by a compression test, a Young's modulus of $115.6 \text{ MPa} \pm 14.6 \text{ MPa}$ and an onset of deformation at around 10 MPa (yield strength) (Fig. 1B, Table 1). The controlled architecture of the scaffolds is analyzed through microscopy and μCT. Pores and struts have reproducible sizes, even at the edges of the scaffold, with an average of $599 \mu\text{m} \pm 28 \mu\text{m}$ and $347 \mu\text{m} \pm 17 \mu\text{m}$ respectively (Fig. 1C–D). The large pores and struts result in a high porosity; about 2/3 of the volume of the scaffold is available for cell/tissue infiltration. However, there are some discrepancies between measurement tools. μCT results in 59.02% ($\pm 2.09\%$) porosity whereas helium pycnometry indicates a porosity of 71.08% ($\pm 3.14\%$) (Table 1). Differences can be explained by resolution limitation of μCT ($8 \times 8 \times 8 \mu\text{m}^3$) and selected cut-off values.

3.2. CAF stimulate 3D cancer cell colonization in PLA scaffolds

PLA scaffolds are 3D colonized by co-seeding luciferase positive cancer cells with human CAF in a suspension of type I collagen (Fig. 2A). Type I collagen, a gel-forming ECM protein, fills the void space in scaffolds and supports 3D growth of cells. Vacuum pressure enables the collagen/cell mixture to reach the center of the scaffolds. Upon gelification, single cells are randomly dispersed in the collagen-occupied voids of the scaffold. Both HCT-8/E11 colon cancer cells (Fig. S1A) and SK-O-V-3 ovarian cancer cells (Fig. 2B) show an initial bioluminescent signal that drops within the first days and starts to recover at the end of week 2. Importantly, co-seeding of cancer cells with CAF surges the initial bioluminescent signal and signal intensity is correlated with increasing CAF numbers. The four-to-one ratio of the number of CAF to the number of cancer cells shows the highest initial bioluminescent signal, which remains stable over a two-week period (Fig. 2B). Scaffolds with the four-to-one ratio were maintained in long-term culture and monitored by phase-contrast microscopy and bioluminescence (Fig. 2C). Within this long-term period, four stages of cellular organization are identified in the scaffolds seeded with a combination of SK-OV-3 and CAF: adhesion/selection, recovery, spheroid formation and exponential growth phase (Fig. 2C); whereas only two

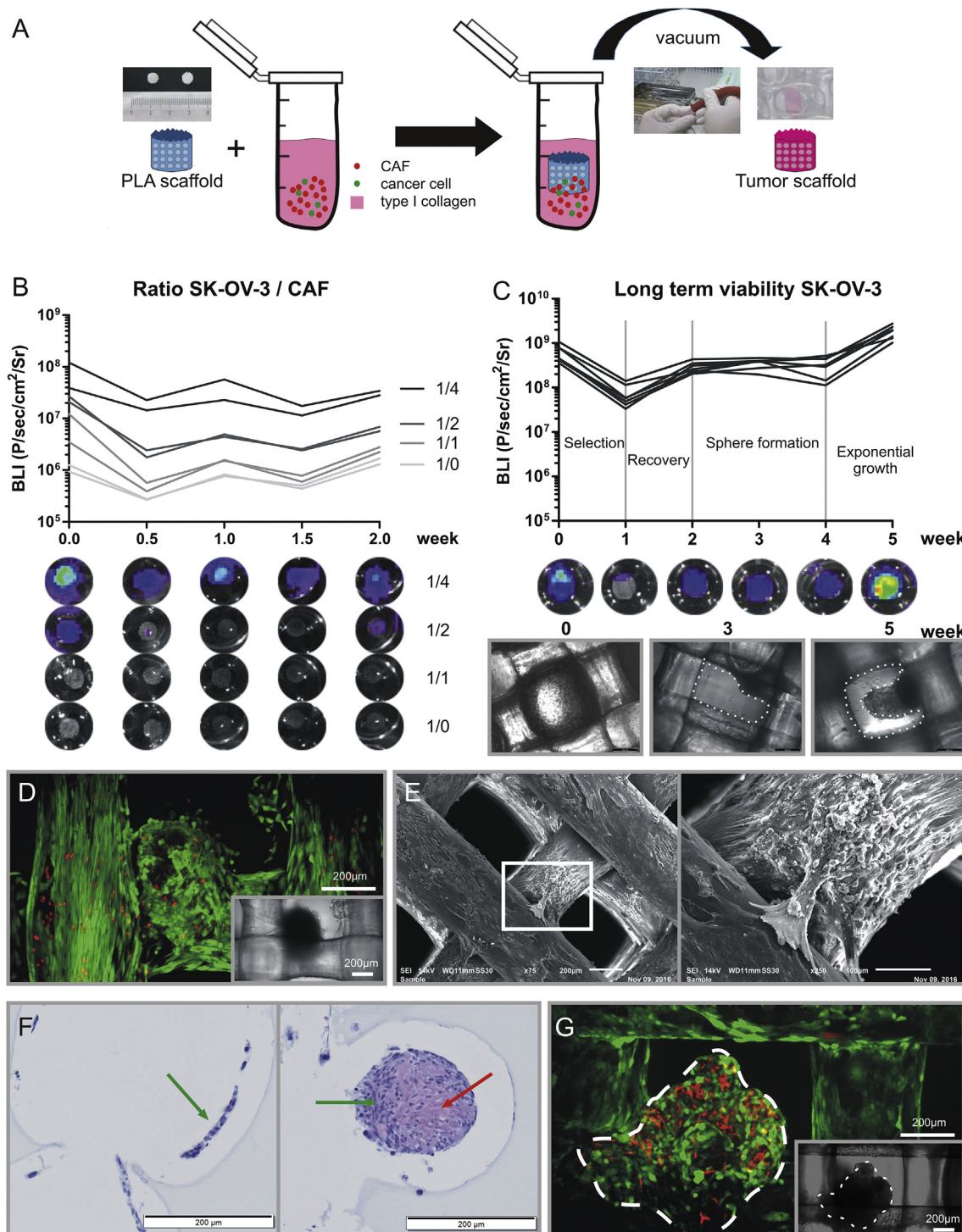


Fig. 2. *In vitro* characterization of ovarian tumor scaffolds. A) Schematic representation of the procedure to seed a combination of extracellular matrix and cells. PLA scaffolds are placed in a mixture of cancer cells and CAF suspended in type I collagen. By applying vacuum pressure, this mixture is drawn into the scaffolds and polymerizes at 37 °C, creating tumor scaffolds. B) Graph (upper panel) and BLI images (lower panel) depicting the viability of 1.5×10^6 SK-OV-3 Luc cells in the scaffolds seeded with increasing numbers of CAF ($n = 4 \times 2$). C) Graph (upper panel), BLI (middle panel) and phase-contrast (lower panel) images of scaffolds seeded with 2×10^6 SK-OV-3 Luc and 8×10^6 CAF at week 0, 3 and 5 ($n = 6$). Hydrogel contraction by CAF reestablish void space within the scaffolds, as indicated by dotted line (not present at baseline). At week 5, LIVE (green)/DEAD (red) staining (D), SEM (E) and H&E staining on microsections (F) were performed. In D) confocal image shows LIVE/DEAD staining while inset shows differential interference contrast (DIC) image at the same position of the confocal image. In E) right panel shows magnification of white rectangular box in left panel. In F) SK-OV-3 Luc and CAF are indicated by green and red arrows respectively. Left and right panel show a monolayer and a spheroid, respectively, originally in contact with PLA scaffold (fixation and staining procedures dissolve PLA). G) Confocal image of a scaffold seeded with 2×10^6 SK-OV-3 Luc eGFP (green) and 8×10^6 CAF tdTomato (red) after 5 weeks of *in vitro* culture. Inset shows phase-contrast image at similar position of confocal image. Dotted line indicates spheroid in both confocal and DIC image. (For interpretation of the references to color in this figure legend, the reader is referred to the Web version of this article.)

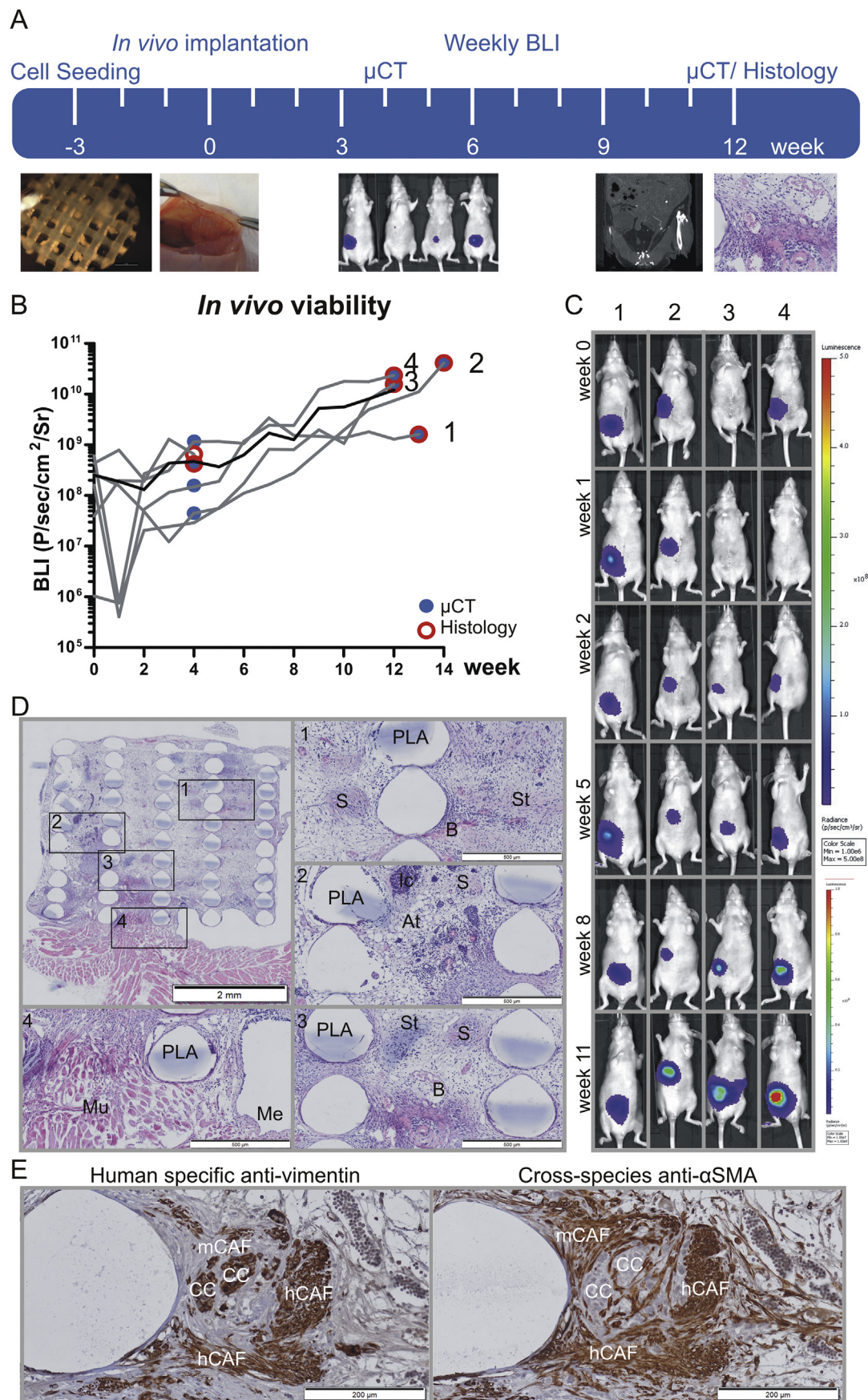


Table 1
Material and scaffold characteristics.

Property	Value	SD
Mn PLA (g/mol)	132400	
MW PLA (p/mol)	166500	
Scaffold diameter (mm)	6.05	0.02
Scaffold height (mm)	4.09	0.02
Volume (mm ³)	117.58	0.623
Pore size (μm)	599	28
Strut thickness (μm)	347	17
E-Modulus (Mpa)	115.6	14.6
Scaffold volume/infill density (μCT) (%)	40.98	2.09
Scaffold volume/infill density (He pycnometry) (%)	28.92	3.14
Volume of voids/porosity (μCT) (%)	59.02	2.09
Volume of voids/porosity (He pycnometry) (%)	71.08	3.14

stages are identified in the scaffolds seeded with a combination of HCT-8/E11 and CAF: adhesion/selection and spheroid formation/exponential growth (Fig. S1B). HCT-8/E11 cells have, in contrast to SK-OV-3 cells, strong E-cadherin-mediated cell-cell adhesion, which is most probably responsible for rapid spheroid formation [25]. LIVE/DEAD staining at week 5 shows high viability of cells both within spheroids and adhered to struts (Fig. 2D). Cells adhered to struts are oriented in the print direction of the scaffold, parallel to the movement of the printing nozzle. Occasionally, cells connecting both a vertical and horizontal strut are observed (Fig. 2E). eGFP expressing SK-OV-3 cells form heterocellular spheroids with tdTomato expressing CAF as well as homocellular monolayers attached to struts. In general, CAF do not grow on struts but are only present within spheroids, making up to 30% of the spheroid cell number. This organization is confirmed by H&E staining of paraffin-embedded sections; basophilic (affinity to haematoxylin) cancer cells are organized into monolayers adhered to struts, whereas spheroids contain both basophilic cancer cells and eosinophilic (affinity to eosin) CAF/matrix (Fig. 2F and G). Similarly, HCT-8/E11 cells not only grow as monolayers attached to struts but also as spheroids, although there is clearly more cancer cell-CAF intermingling in spheroids with SK-OV-3 cancer cells than occurs with HCT-8/E11 cancer cells. In fact, HCT-8/E11 spheroids have a central core of HCT-8/E11 cancer cells, surrounded by a CAF-rich matrix (Fig. S1C). Above all, bioluminescence imaging, fluorescence microscopy and histological data show that CAF are essential for cancer cell colonization and formation of a tumor scaffold *in vitro*.

3.3. *In vivo* evaluation of tumor scaffolds and infiltrated cells

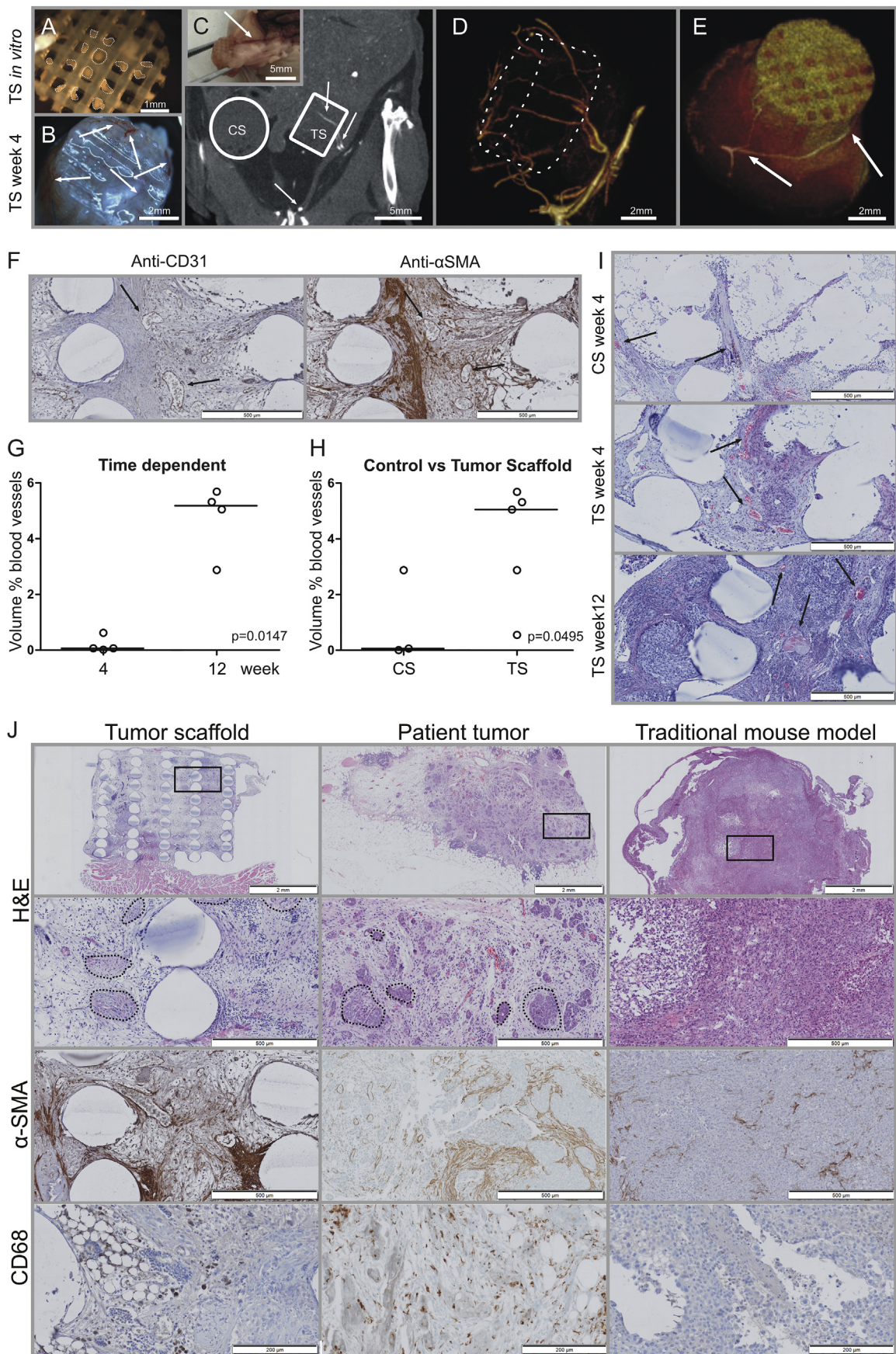
We further explored whether tumor scaffolds could be used as an orthotopic peritoneal metastasis model. Tumor scaffolds were maintained *in vitro* for 3 weeks prior to surgical implantation to the peritoneal wall at the right lower quadrant of the peritoneal cavity. This time window is crucial for the cancer cells to recover and to form spheroids (microscopic Fig. 2C bottom panel; macroscopic Fig. 3A). Interestingly, phase-contrast microscopy reveals that type I collagen hydrogels are initially intact, but then contract over time, most likely through CAF-mediated contractile activity, resulting in the creation of voids within the scaffolds, which in turn allows

space for both host cell infiltration and vascularization *in vivo* (Fig. 2C). In 4 out of 6 mice, a control scaffold (collagen-PLA [gel-MOD]; no cells) was added to the left lower quadrant. The bioluminescent activity of the cancer cells in the scaffolds was longitudinally monitored. In 3 out of 6 mice, a steep decrease in bioluminescent signal in the first week after implantation was observed, which showed recovery by the second week (Fig. 3B–C). This could reflect a temporal drop in cancer cell viability or an insufficient distribution of the luciferin within the scaffold. Long-term follow-up reveals an exponential increase of a localized bioluminescent signal at the scaffold implantation area. At 4 weeks post implantation, the scaffolds contain clusters of cancer cells and CAF surrounded by mouse fibroblasts, adipocytes, inflammatory cells and endothelial cells, forming heterogeneous tumor tissue. At the intersection between the scaffold and the peritoneal wall, an intimate interaction between the tumor and the muscle cells is observed (Fig. 3D). Mesothelial cells do not cover the scaffold. Immunohistochemical staining with a human specific anti-vimentin antibody and a cross-species anti- αSMA antibody indicates the presence of infiltrating mouse CAF surrounding cancer cells and human co-seeded CAF (Fig. 3E). Blood vessels are clearly visible on the H&E sections (Fig. 3D); the wide distribution of blood vessels throughout the scaffold is in agreement with the absence of necrotic areas. The area of blood vessels correlates ($R = 1$, $p = .0083$) with the bioluminescent signal of the cancer cells in the scaffold (Fig. S2B). Peri- and intra-tumor scaffold vascularization is evidenced by *ex vivo* macroscopic evaluation (Fig. 4A–B shows pre- and post-implanted scaffolds) and contrast-enhanced μCT both *in vivo* (Fig. 4C–D) and *ex vivo* (Fig. 4E). Tissue sections of the scaffold show that CD31 positive vessels are covered by αSMA positive pericytes (Fig. 4F). Peri-tumor scaffold branching of vessels is observed *ex vivo* macroscopically and *in vivo* using μCT . Video 1 demonstrates a blood vessel following the inner lining of the peritoneal wall until the tumor scaffold, where it bends 90° to enter the scaffold. Video 2 is a 3D reconstruction of the same tumor scaffold. Contrast-enhanced μCT shows a 15-fold increase ($p = .0147$) in the blood vessel volume in an 8-week time period (week 4: 0.06 vol % blood vessel (IQR = 0.03–0.48), week 12: 5.18 vol % blood vessel (IQR = 3.42–5.60)) (Fig. 4G). Tissue exposure to biomaterials triggers a foreign body response (FBR) characterized by inflammatory cell recruitment and fibrosis-induced vessel regression. To evaluate the FBR to PLA scaffolds, control scaffolds were peritoneally implanted. H&E staining shows that control scaffolds are infiltrated by inflammatory cells, fibroblasts and small blood vessels. Although blood vessels are present, robust neovascularization is not observed since the blood vessel volume percentage is 3.97-fold lower ($p = .0495$) in control scaffolds (0.06 vol % blood vessel (IQR = 0.008–2.88)) compared to tumor scaffolds (5.05 vol % blood vessel (IQR = 1.71–5.50)) (Fig. 4G–H). This suggests an active and sustained cancer cell/CAF-dependent recruitment and organization of blood vessels in tumor scaffolds.

Supplementary data related to this article can be found online at <https://doi.org/10.1016/j.biomaterials.2017.12.017>

To further demonstrate that tumor scaffolds actively recruit host cells and do not only elicit an FBR to the biomimetic construct, we

Fig. 3. *In vivo* biomimetic of ovarian peritoneal metastases. A) Schematic timeline of the *in vivo* experiments. The collagen/cell mixture was seeded in PLA scaffolds 3 weeks prior to *in vivo* implantation of tumor scaffolds. Mice were monitored weekly by BLI (B, C) ($n = 6$). Contrast-enhanced μCT (week 4 and 12) and histology (end-point) were performed (D, E). Weekly BLI results of individual mice are indicated in a graph (B) with an indication when μCT and end-point histology were performed. Gray lines represent individual mice, whereas the black line is the average BLI. C) BLI images of four individual mice monitored over 11 weeks. D) H&E staining of a tumor scaffold 4 weeks post implantation with human specific anti-vimentin visualizes human cells only (*i.e.* seeded cells) and with cross-species anti- αSMA visualizes both host cells and seeded αSMA positive cells. CC; Cancer cells are human vimentin positive and αSMA negative. hCAF; Human CAF are human vimentin and αSMA positive. mCAF; Mouse CAF are human vimentin negative and αSMA positive.



compared the histological organization of 1) a peritoneally implanted SK-OV-3 tumor scaffold, 2) a patient-derived ovarian cancer peritoneal metastasis removed during cytoreductive surgery and 3) an ovarian xenograft tumor obtained by intraperitoneal injection of SK-OV-3 single cell suspension (traditional xenograft) (Fig. 4). The heterocellular nature of the tumor scaffold is similar to what we observe in patient samples: nests of cancer cells surrounded by stroma. This morphology resembles the cancer cell/CAF spheroid formation in the tumor scaffolds. Tumor scaffolds and patient-derived samples abundantly contain pericyte-covered (α SMA positive) blood vessels, whereas intraperitoneally injected SK-OV-3 cells form small peritoneal metastases with only occasional blood vessels. The organization of α SMA positive fibroblasts is different between traditional xenografts and patient-derived samples/tumor scaffolds. In traditional xenografts, occasional α SMA positive fibroblasts tightly adhere to the periphery of SK-OV-3 nests in one to three layers. In tumor scaffolds and patient-derived samples, however, α SMA positive fibroblasts are arranged in a multilayered network pattern in close contact with cancer cells. Furthermore, numbers of CAF occasionally exceed those of cancer cells. Inflammation, an intricate part of tumor progression, is characterized by presence of CD68 positive macrophages in tumor scaffolds and patient samples. However, CD68 positive macrophages are not observed in traditional SK-OV-3 xenografts. In conclusion, peritoneally implanted SK-OV-3 tumor scaffolds and patient-derived tumor tissue show a similar morphological, blood vessel and (α SMA positive) fibroblast organization as well as (CD68 positive) macrophage infiltration.

An FBR to a cell-free/control scaffold is characterized by infiltration of host cells similar like those observed in a tumor scaffold, but to a spatial different and quantitative lesser extent. To understand why tumor scaffolds more truthfully mimic a patient-derived peritoneal metastasis compared to intraperitoneal injection of SK-OV-3 cells or an FBR to the hybrid hydrogel-PLA scaffold, we decided to investigate the secretome of both cancer cells and CAF. Secretory products such as chemokines, cytokines and growth factors serve paracrine communication with the host and are responsible for tumor infiltration of macrophages, endothelial cells, fibroblasts and pericytes. While some growth factors/cytokines/chemokines are similarly secreted by both cancer cells and CAF (CXCL10, GRO α , VEGF-A, angiopoietin-2, FGF-2, IL-8, IFN α 2), others are uniquely secreted by the cancer cells (CX3CL1, eotaxin-2, MIP-1 α , Rantes, MDC, LIF, IL-28a, IL-1a, TGF α , GM-CSF, PDGF-AA, PDGF-BB, SCF, TNF α , HB-EGF, PLGF) and others are uniquely secreted by the CAF (eotaxin-1, MCP-1, MCP-2, MCP-3, MCP-4, SDF-1a&b, ENA-78, IL-15, IL-6, IL-23, Flt-3L, endoglin, follistatin, SF/HGF, VEGF-C) (Fig. S3 and Table S1). Thus, the complementary secretory profile of growth factors/chemokines/cytokines by both cancer cells and CAF is most probably responsible for recruitment and organization of host cells in tumor scaffolds as similarly observed in ovarian cancer patient-derived peritoneal metastases.

4. Discussion

Key features of the design include a type I collagen hydrogel to imbibe and trap cells in a gel phase, and vacuum pressure to allow distribution of the cell-laden hydrogel throughout all pores of the network. Notably, in the absence of the collagen hydrogel, cells flow through the pores network of the scaffold without adhering to the PLA substrate, even though it was activated by argon plasma treatment and subsequently coated with gel-MOD. Furthermore, PLA scaffolds can be designed into any desired size and shape with relatively high mechanical strength and they can be sutured onto biological surfaces such as the peritoneum. Peritoneal metastases are dome-shaped elevations on the peritoneal surface and their size is of clinical importance since intraperitoneal chemotherapy has limited survival benefit in patients with peritoneal metastases exceeding the size of 5.0 mm for ovarian cancer [4] and 2.5 mm for colon cancer [5]. The established technology of FDM enables manufacture of peritoneal metastases with tunable properties, such as weight, size and shape, being therefore superior to traditional peritoneal metastasis models in terms of (clinically relevant) spatial dimensions.

Since solid tumors are more than a mass of genetically altered cells (*i.e.* the cancer cells), scaffolds were co-seeded with cancer cells and fibroblasts, which are abundantly present in the tumor microenvironment (*i.e.* so-called cancer-associated fibroblasts, CAF). Interestingly, in absence of CAF, cancer cells (both ovarian SK-OV-3 and colorectal HCT-8/E11 cells) prefer to adhere to and grow on the scaffolds' struts, suggesting 2D growth on a 3D substrate. CAF, however, promote the formation of heterocellular spheroids within the hydrogel-occupied pores of the scaffold, a process strongly dependent upon the CAF seeding number. Indeed, spheroid formation is profoundly influenced by CAF through paracrine signaling [26–28]. Furthermore, Chen et al. found that CAF-induced spheroid formation led to the sustaining of cancer cell stemness [27]. In ovarian cancer, there is strong evidence that spheroids originating from malignancy-related ascites exhibit increased tumorigenic capacity *in vivo*, potentially seed metastatic lesions and could be correlated with therapy resistance [29,30]. Besides spheroid formation, we have observed a significant difference in cancer cell viability; all CAF seeding numbers increased cancer cell survival, an effect that exponentially increased with increasing CAF numbers. This is consistent with prior related *in vitro* studies that have shown increased viability of cancer cells co-cultured with CAF. In these studies, the fibroblast-mediated increase in viability was attributable to growth factors and chemokines such as SF/HGF, NRG1, SDF1, among others [20,31,32]. CAF support tumorigenesis through various mechanisms, including cancer cell stemness, proliferation, invasion and angiogenesis. Furthermore, clinical data demonstrated that stromal characteristics, such as the carcinoma-stroma ratio [33–37] and the stromal gene signature [38,39], can predict patient survival and are

Fig. 4. Blood vessel infiltration. Stereomicroscopic images of a tumor scaffold before implantation (at week 0) (A) and at week 4 post implantation (B). In A) dotted lines indicate spheroids and in B) arrows indicate blood vessels. C) Contrast-enhanced μ CT images of a mouse implanted with a cell-free/control scaffold (CS) and tumor scaffold (TS) 4 weeks post implantation. Scaffolds are differently orientated. The arrows indicate the blood vessels infiltrating the tumor scaffold. This was confirmed by *post mortem* analysis, as can be seen in the insert (same tumor scaffold). D) 3D reconstruction of the blood vessels surrounding and infiltrating the same tumor scaffold. Dotted line indicates position of tumor scaffold. E) Contrast-enhanced μ CT 3D reconstruction of an *ex vivo* tumor scaffold. Arrow indicates infiltrating blood vessel. Tissue (red) has a lower density than the PLA scaffold (yellow). F) Immunohistochemistry was performed on a tumor scaffold 4 weeks post implantation by using anti-CD31 antibodies (endothelial cells) and anti- α SMA antibodies (CAF and pericytes). Both proteins are markers for mature blood vessels, which are indicated with an arrow. G) and H) Quantification of infiltrating blood vessels on contrast-enhanced μ CT images. Volume percent blood vessels is calculated by using: (volume infiltrated blood vessels/volume scaffold) \times 100. The volume of blood vessels in tumor scaffolds increases over time (G) and tumor scaffolds have a higher volume of infiltrating blood vessels compared to control scaffolds (H). I) H&E staining of a cell-free/control scaffold 4 weeks post implantation and tumor scaffold 4 and 12 weeks post implantation. Arrows indicate blood vessels. J) H&E and immunohistochemical stainings of an ovarian tumor scaffold (4 weeks post implantation), a patient-derived ovarian cancer peritoneal metastasis removed during cytoreductive surgery and a mouse xenograft tumor obtained by intraperitoneal injection of SK-OV-3 Luc cells. Black rectangular boxes indicate area of magnification on the overview slide. Dotted lines indicate epithelial nests embedded in stroma. Anti- α SMA visualizes human and mouse CAF as well as pericytes covering endothelial cells of functional blood vessels. Anti-CD68 visualizes human and mouse macrophages. (For interpretation of the references to color in this figure legend, the reader is referred to the Web version of this article.)

correlated with poor prognosis.

An FBR is mainly mediated by macrophages as inducers of fibrotic encapsulation via VEGF release and neovascularization [18]. Accordingly, an FBR is likely to occur in T and B cell immunodeficient mice commonly used in xenograft models. An FBR is in general undesirable and can be deleterious to the function of the implanted tumor scaffold. Several aspects indicate that the host cell response to the implanted tumor scaffold is not merely an FBR but an active, controlled recruitment of host cells by paracrine factors produced by the tumor scaffold. Firstly, rapid contraction of collagen hydrogels *in vitro* is the result of contractile forces generated by CAF, which in turn determines the new tissue formation *in vivo* by allowing space and structural support for host cell infiltration and vascularization. Secondly, the scaffolds were maintained up to 14 weeks without the appearance of thick fibrotic tissue at the contact area between the implanted scaffold and the host. In contrast, a typical FBR occurs within 4 weeks after scaffold implantation. Thirdly, blood vessel infiltration correlates with growth and viability of cancer cells in the tumor scaffold. Fourthly, a control scaffold without cells shows a 4-fold lower neovascularization compared to a tumor scaffold. This highlights the importance of cancer cell/CAF-derived paracrine factors in the recruitment of pericyte-covered (α SMA positive) CD31 expressing endothelial cells. Fifthly, cancer cells and CAF produce a complementary cocktail of factors implicated in the stimulation of neovascularization. While macrophage-derived VEGF is mainly the initiator of an FBR, tumor scaffolds produce VEGF supplemented with pro-angiogenic factors such as PDGF family members, SF/HGF, PLGF, among others. Sixthly, the complementary pro-angiogenic cocktail that shows a sustained release (data not shown) is most probably responsible for the 15-fold increase in blood vessel volume over an 8-week time period. And lastly, CD68 positive macrophages did not accumulate at the scaffold-host interface but showed close association with cancer cell nests as is similarly observed in a patient-derived peritoneal metastasis.

An important aspect is whether the tumor hybrid scaffold is superior to traditional tumor models in preclinical drug testing. A commonly used model is the intraperitoneal injection of a cancer cell suspension, which simulates the process of peritoneal dissemination in intra-abdominal cancers. However, it is difficult to achieve heterologous growth of human cancer cell lines in the abdominal cavity of nude mice by direct intraperitoneal injection due to the acute conversion from an adherent-dependent to a suspension-dependent type of survival of the human cancer cells. Direct intraperitoneal injection of 1×10^6 SK-OV-3 cells in nude mice results in a long latency and in a small number of palpable tumor nodes [10]. Histological analysis revealed necrotic areas and minimal stromal contribution of both CAF and blood vessels to tumorigenesis in this traditional peritoneal metastasis model. This stands in stark contrast with a patient-derived peritoneal metastasis showing abundant stromal components intermingled between multicellular clusters of cancer cells. Of interest, tumor scaffolds implanted on the peritoneum are histologically similar to native tumor tissue; in addition to multicellular clusters of cancer cells, they also contain a multilayered network composed of α SMA positive fibroblasts, a pericyte-stabilized vascular network and infiltrating immune cells.

Models that truthfully mimic peritoneal metastases are important for the preclinical evaluation of intraperitoneal drug delivery [40]. The uptake of both low-molecular-weight and high-molecular-weight drugs is strongly influenced by stromal-environmental factors in peritoneal metastases. Peritoneal metastases have a raised interstitial fluid pressure due to stiff stroma (established by extracellular matrix-producing CAF) and leaky blood vessels [41,42]. In addition, there are several reports on chemotherapy

scavenging of CAF, thus reducing the availability of these drugs to nearby cancer cells. The tumor scaffold model in this study differs from most peritoneal metastasis models, because of its consistency in size and the marked histological similarity to patient-derived peritoneal metastases. Furthermore, this model allows the longitudinal use of advanced *in vivo* techniques (bioluminescence and μ CT). Lastly, specific size-dependent aspects of tumor biology such as oxygenation, perfusion and interstitial fluid pressure may be evaluated more accurately.

In conclusion, we have tissue-engineered and characterized a new implantable scaffold model based on the human tumor microenvironment. Our findings underscore that CAF enhance both cancer cell survival and angiogenesis by offering a privileged environment. Our approach describes another step forward in recapitulating the multifaceted tumor microenvironment by increasing complexity of tissue-engineered tumor models. It is likely that the scaffold model could be further developed as a platform technology that may enable mechanistic studies for drug penetration and efficacy after intraperitoneal chemotherapy delivery.

Acknowledgements

This research was supported by Research Council of Ghent University (BOF) and grants from "Kom op tegen Kanker", "Stichting tegen Kanker", Cancer Research Institute Ghent (CRIG) and the European Research Council.

Appendix A. Supplementary data

Supplementary data related to this article can be found at <https://doi.org/10.1016/j.biomaterials.2017.12.017>.

References

- [1] W.P. Ceelen, M.F. Flessner, Intraperitoneal therapy for peritoneal tumors: biophysics and clinical evidence, *Nat. Rev. Clin. Oncol.* 7 (2010) 108–115, <https://doi.org/10.1038/nrclinonc.2009.217>.
- [2] V.J. Verwaal, S. van Ruth, E. de Bree, G.W. van Slooten, H. van Tinteren, H. Boot, et al., Randomized trial of cytoreduction and hyperthermic intraperitoneal chemotherapy versus systemic chemotherapy and palliative surgery in patients with peritoneal carcinomatosis of colorectal cancer, *J. Clin. Oncol.* 21 (2003) 3737–3743, <https://doi.org/10.1200/JCO.2003.04.187>.
- [3] D.K. Armstrong, B. Bundy, L. Wenzel, H.Q. Huang, R. Baergen, S. Lele, et al., Intraperitoneal cisplatin and paclitaxel in ovarian cancer, *N. Engl. J. Med.* 354 (2006) 34–43, <https://doi.org/10.1056/NEJMoa052985>.
- [4] R.R. Barakat, P. Sabatini, D. Bhaskaran, M. Revzin, A. Smith, E. Venkatraman, et al., Intraperitoneal chemotherapy for ovarian carcinoma: results of long-term follow-up, *J. Clin. Oncol.* 20 (2002) 694–698. <http://www.ncbi.nlm.nih.gov/pubmed/11821450>.
- [5] D. Elias, F. Gilly, F. Boutitie, F. Quenet, J.-M. Bereder, B. Mansvelt, et al., Peritoneal colorectal carcinomatosis treated with surgery and perioperative intraperitoneal Chemotherapy : retrospective analysis of 523 patients from a multicentric French study, *J. Clin. Oncol.* 28 (2010) 63–68, <https://doi.org/10.1200/JCO.2009.23.9285>.
- [6] C. Carlier, A. Mathys, E. De Jaeghere, M. Steuperaert, O. De Wever, W. Ceelen, Tumour tissue transport after intraperitoneal anticancer drug delivery, *Int. J. Hyperth.* 33 (2017) 534–542, <https://doi.org/10.1080/02656736.2017.1312563>.
- [7] C. Carlier, B. Laforce, S.J.M. Van Malderen, F. Gremont, R. Tucoulou, J. Villanova, et al., Nanoscopic tumor tissue distribution of platinum after intraperitoneal administration in a xenograft model of ovarian cancer, *J. Pharm. Biomed. Anal.* 131 (2016) 256–262, <https://doi.org/10.1016/j.jpba.2016.09.004>.
- [8] F. Gremont, W. Willaert, W. Ceelen, Intraperitoneal chemotherapy (IPC) for peritoneal carcinomatosis: review of animal models, *J. Surg. Oncol.* 109 (2014) 110–116, <https://doi.org/10.1002/jso.23464>.
- [9] E. De Vlieghere, F. Gremont, L. Verset, L. Mariën, C.J. Jones, B. De Craene, et al., Tumor-environment biomimetics delay peritoneal metastasis formation by deceiving and redirecting disseminated cancer cells, *Biomaterials* 54 (2015) 148–157, <https://doi.org/10.1016/j.biomaterials.2015.03.012>.
- [10] E. De Vlieghere, C. Carlier, W. Ceelen, M. Bracke, O. De Wever, Data on *in vivo* selection of SK-OV-3 Luc ovarian cancer cells and intraperitoneal tumor formation with low inoculation numbers, *Data Bus.* 6 (2016) 542–549, <https://doi.org/10.1016/j.biomaterials.2015.03.012>.

- [doi.org/10.1016/j.dib.2015.12.037.](https://doi.org/10.1016/j.dib.2015.12.037)
- [11] M.R. Kuracha, P. Thomas, B.W. Loggie, V. Govindarajan, Patient-derived xenograft mouse models of pseudomyxoma peritonei recapitulate the human inflammatory tumor microenvironment, *Cancer Med* 5 (2016) 711–719, <https://doi.org/10.1002/cam4.640>.
- [12] F. Gremonprez, B. Descamps, A. Izmer, C. Vanhove, F. Vanhaecke, O. De Wever, et al., Pretreatment with VEGF (R)-inhibitors reduces interstitial fluid pressure, increases intraperitoneal chemotherapy drug penetration, and impedes tumor growth in a mouse colorectal carcinomatosis model, *Oncotarget* 6 (2015), <https://doi.org/10.18632/oncotarget.5092>.
- [13] C. Carlier, S. Streste, K. Viktorsson, E. Velander, P. Nygren, M. Uustalu, et al., Preclinical activity of melflufen (J1) in ovarian cancer, *Oncotarget* (2016), <https://doi.org/10.18632/oncotarget.11163>.
- [14] W. Bouquet, S. Deleye, S. Staelens, L. De Smet, N. Van Damme, I. Debergh, et al., Antitumour efficacy of two paclitaxel formulations for hyperthermic intraperitoneal chemotherapy (HIPEC) in an *in vivo* rat model, *Pharm. Res.* 28 (2011) 1653–1660, <https://doi.org/10.1007/s11095-011-0401-1>.
- [15] M.A. Swartz, N. Iida, E.W. Roberts, S. Sangaletti, M.H. Wong, F.E. Yull, et al., Tumor microenvironment complexity: emerging roles in cancer therapy, *Cancer Res.* 72 (2012) 2473–2480, <https://doi.org/10.1158/0008-5472.CAN-12-0122>.
- [16] B.A. Aguado, G.G. Bushnell, S.S. Rao, J.S. Jeruss, L.D. Shea, Engineering the pre-metastatic niche, *Nat. Biomed. Eng.* 1 (2017) 77, <https://doi.org/10.1038/s41551-017-0077>.
- [17] L.C. Martine, B.M. Holzapfel, J.A. McGovern, F. Wagner, V.M. Quent, P. Hesami, et al., Engineering a humanized bone organ model in mice to study bone metastases, *Nat. Protoc.* 12 (2017) 639–663, <https://doi.org/10.1038/nprot.2017.002>.
- [18] E. Dondossola, B.M. Holzapfel, S. Alexander, S. Filippini, D.W. Hutmacher, P. Friedl, Examination of the foreign body response to biomaterials by nonlinear intravital microscopy, *Nat. Biomed. Eng.* 1 (2016) 7, <https://doi.org/10.1038/s41551-016-0007>.
- [19] L. Zhao, G. Ji, X. Le, C. Wang, L. Xu, M. Feng, et al., Long noncoding RNA LINC0092 acts in cancer-associated fibroblasts to drive glycolysis and progression of ovarian cancer, *Cancer Res.* 77 (2017) 1369–1382, <https://doi.org/10.1158/0008-5472.CAN-16-1615>.
- [20] O. De Wever, Q.-D. Nguyen, L. Van Hoorde, M. Bracke, E. Bruyneel, C. Gespach, et al., Tenascin-C and SF/HGF produced by myofibroblasts in vitro provide convergent pro-invasive signals to human colon cancer cells through RhoA and Rac, *J. Cell. Sci.* 118 (2004) 1016–1018, <https://doi.org/10.1096/fj.03-1110fje>.
- [21] J. Van Hoorick, H. Declercq, A. De Muynck, A. Houben, L. Van Hoorebeke, R. Cornelissen, et al., Indirect additive manufacturing as an elegant tool for the production of self-supporting low density gelatin scaffolds, *J. Mater. Sci. Mater. Med.* 26 (2015), <https://doi.org/10.1007/s10856-015-5566-4>.
- [22] T. Desmet, T. Billiet, E. Berneel, R. Cornelissen, D. Schaubroeck, E. Schacht, et al., Post-plasma grafting of AEMA as a versatile tool to biofunctionalise polyesters for tissue engineering, *Macromol. Biosci.* 10 (2010) 1484–1494, <https://doi.org/10.1002/mabi.201000147>.
- [23] A. De Boeck, A. Hendrix, D. Maynard, M. Van Bockstal, A. Daniëls, P. Pauwels, et al., Differential secretome analysis of cancer-associated fibroblasts and bone marrow-derived precursors to identify microenvironmental regulators of colon cancer progression, *Proteomics* 13 (2013) 379–388, <https://doi.org/10.1002/pmic.201200179>.
- [24] O. De Wever, A. Hendrix, A. De Boeck, W. Westbroek, G. Braems, S. Emami, et al., Modeling and quantification of cancer cell invasion through collagen type I matrices, *Int. J. Dev. Biol.* 54 (2010) 887–896, <https://doi.org/10.1387/ijdb.092948ow>.
- [25] S.J. Vermeulen, E.A. Bruyneel, M.E. Bracke, G.K. De Bruyne, K.M. Vennekens, K.L. Vleminckx, et al., Transition from the noninvasive to the invasive phenotype and loss of alpha-catenin in human colon cancer cells, *Cancer Res.* 55 (1995) 4722–4728, <http://www.ncbi.nlm.nih.gov/pubmed/7553655> (Accessed August 21 2017).
- [26] S.Y. Jeong, J.H. Lee, Y. Shin, S. Chung, H.J. Kuh, Co-culture of tumor spheroids and fibroblasts in a collagen matrix-incorporated microfluidic chip mimics reciprocal activation in solid tumor microenvironment, *PLoS One* 11 (2016) 1–17, <https://doi.org/10.1371/journal.pone.0159013>.
- [27] W.-J. Chen, C.-C. Ho, Y.-L. Chang, H.-Y. Chen, C.-A. Lin, T.-Y. Ling, et al., Cancer-associated fibroblasts regulate the plasticity of lung cancer stemness via paracrine signalling, *Nat. Commun.* 5 (2014) 1–17, <https://doi.org/10.1038/ncomms4472>.
- [28] C.-P. Liao, H. Adisetiyo, M. Liang, P. Roy-Burman, Cancer-associated fibroblasts enhance the gland-forming capability of prostate cancer stem cells, *Cancer Res.* 70 (2010) 7294–7303, <https://doi.org/10.1158/0008-5472.CAN-09-3982>.
- [29] J. Liao, F. Qian, N. Tchabo, P. Mhawech-Fauceglia, A. Beck, Z. Qian, et al., Ovarian cancer spheroid cells with stem cell-like properties contribute to tumor generation, metastasis and chemotherapy resistance through hypoxia-resistant metabolism, *PLoS One* 9 (2014), <https://doi.org/10.1371/journal.pone.0084941> e84941.
- [30] H.J. Allen, C. Porter, M. Gamarra, M.S. Piver, E.A. Johnson, Isolation and morphologic characterization of human ovarian carcinoma cell clusters present in effusions, *Exp. Cell Biol.* 55 (1987) 194–208, <http://www.ncbi.nlm.nih.gov/pubmed/3678576> (Accessed August 31 2017).
- [31] A. De Boeck, P. Pauwels, K. Hensen, J.-L. Rummens, W. Westbroek, A. Hendrix, et al., Bone marrow-derived mesenchymal stem cells promote colorectal cancer progression through paracrine neuregulin 1/HER3 signalling, *Gut* 62 (2013) 550–560, <https://doi.org/10.1136/gutjnl-2011-301393>.
- [32] A. Orimo, P.B. Gupta, D.C. Sgroi, F. Arenzana-Seisdedos, T. Delaunay, R. Naeem, et al., Stromal fibroblasts present in invasive human breast carcinomas promote tumor growth and angiogenesis through elevated SDF-1/CXCL12 secretion, *Cell* 121 (2005) 335–348, <https://doi.org/10.1016/j.cell.2005.02.034>.
- [33] W.E. Mesker, J.M.C. Junggeburt, K. Szuhai, P. de Heer, H. Morreau, H.J. Tanke, et al., The carcinoma-stromal ratio of colon carcinoma is an independent factor for survival compared to lymph node status and tumor stage, *Cell. Oncol.* 29 (2007) 387–398, <http://www.ncbi.nlm.nih.gov/pubmed/17726261> (Accessed August 31 2017).
- [34] N.P. West, M. Dattani, P. McShane, G. Hutchins, J. Grabsch, W. Mueller, et al., The proportion of tumour cells is an independent predictor for survival in colorectal cancer patients, *Br. J. Canc.* 102 (2010) 1519–1523, <https://doi.org/10.1038/sj.bjc.6605674>.
- [35] E.F.W. Courrech Staal, M.W.J.M. Wouters, J.W. van Sandick, M.M. Takkenberg, V.T.H.B.M. Smit, J.M.C. Junggeburt, et al., The stromal part of adenocarcinomas of the oesophagus: does it conceal targets for therapy?, *Eur. J. Cancer* 46 (2010) 720–728, <https://doi.org/10.1016/j.ejca.2009.12.006>.
- [36] A. Labiche, N. Heutte, P. Herlin, J. Chasle, P. Gauduchon, N. Elie, Stomal compartment as a survival prognostic factor in advanced ovarian carcinoma, *Int. J. Gynecol. Canc.* 20 (2010) 28–33, <https://doi.org/10.1111/IGC.0b013e3181bda1cb>.
- [37] H. Panayiotou, N.M. Orsi, H.H. Thygesen, A.I. Wright, M. Winder, R. Hutson, et al., The prognostic significance of tumour-stroma ratio in endometrial carcinoma., *BMC Canc.* 15 (2015) 955, <https://doi.org/10.1186/s12885-015-1981-7>.
- [38] G. Finak, N. Bertos, F. Pepin, S. Sadekova, M. Souleimanova, H. Zhao, et al., Stromal gene expression predicts clinical outcome in breast cancer, *Nat. Med.* 14 (2008) 518–527, <https://doi.org/10.1038/nm1764>.
- [39] P. Farmer, H. Bonnefoi, P. Anderle, D. Cameron, P. Wirapati, P. Wirapati, et al., A stroma-related gene signature predicts resistance to neoadjuvant chemotherapy in breast cancer, *Nat. Med.* 15 (2009) 68–74, <https://doi.org/10.1038/nm1908>.
- [40] M. Stadler, S. Walter, A. Walzl, N. Kramer, C. Unger, M. Scherzer, et al., Increased complexity in carcinomas: analyzing and modeling the interaction of human cancer cells with their microenvironment, *Semin. Canc. Biol.* 35 (2015) 107–124, <https://doi.org/10.1016/j.semcancer.2015.08.007>.
- [41] R. Kalluri, The biology and function of fibroblasts in cancer., *Nat. Rev. Cancer* 16 (2016) 582–598, <https://doi.org/10.1038/nrc.2016.73>.
- [42] C.-H. Heldin, K. Rubin, K. Pietras, A. Östman, High interstitial fluid pressure – an obstacle in cancer therapy, *Nat. Rev. Cancer* 4 (2004) 806–813, <https://doi.org/10.1038/nrc1456>.